^{124}I-huA33 Antibody Uptake Is Driven by A33 Antigen Concentration in Tissues from Colorectal Cancer Patients Imaged by Immuno-PET

Joseph A. O'Donoghue[1], Peter M. Smith-Jones[2], John L. Humm[1], Shutian Ruan[2], Daniel A. Pryma[2], Achim A. Jungbluth[3], Chaitanya R. Divgi[2], Jorge A. Carrasquillo[2], Neeta Pandit-Taskar[2], Yuman Fong[4], Vivian E. Strong[4], Nancy E. Kemeny[5], Lloyd J. Old[3], and Steven M. Larson[2]

[1]Department of Medical Physics, Memorial Sloan-Kettering Cancer Center, New York, New York; [2]Department of Radiology, Memorial Sloan-Kettering Cancer Center, New York, New York; [3]Ludwig Institute for Cancer Research (New York Branch), Memorial Sloan-Kettering Cancer Center, New York, New York; [4]Department of Surgery, Memorial Sloan-Kettering Cancer Center, New York, New York; and [5]Department of Medicine, Memorial Sloan-Kettering Cancer Center, New York, New York

The primary aim of this analysis was to examine the quantitative features of antibody–antigen interactions in tumors and normal tissue after parenteral administration of antitumor antibodies to human patients. **Methods:** Humanized anti-A33 antibody (10 mg) labeled with the positron-emitting radionuclide ^{124}I (^{124}I-huA33) was injected intravenously in 15 patients with colorectal cancer. Clinical PET/CT was performed approximately 1 wk later, followed by a detailed assay of surgically removed tissue specimens including radioactivity counting, autoradiography, immunohistochemistry, and antigen density determination. **Results:** PET/CT showed high levels of antibody targeting in tumors and normal bowel. In tissue specimens, the spatial distribution of ^{124}I-huA33 conformed to that of A33 antigen, and there was a linear relationship between the amount of bound antibody and antigen concentration. Antibody uptake was high in 1- to 2-mm regions of antigen-positive tumor cells (mean, ~0.05 percentage injected dose per gram) and in antigen-positive normal colonic mucosa (mean, ~0.03 percentage injected dose per gram). The estimated binding site occupancy for tumor and normal colon was 20%–50%. **Conclusion:** The in vivo biodistribution of ^{124}I-huA33 in human patients 1 wk after antibody administration was determined by A33 antigen expression. Our data imply that the optimal strategy for A33-based radioimmunotherapy of colon cancer will consist of a multistep treatment using a radionuclide with short-range (α- or β-particle) emissions.

Key Words: huA33; colorectal cancer; ^{124}I; immuno-PET; radioimmunotherapy

J Nucl Med 2011; 52:1878–1885
DOI: 10.2967/jnumed.111.095596

A33 is a cell surface glycoprotein abundantly expressed in 95% of colon carcinomas and by epithelial cells of the normal intestine but not by other normal tissues (*1–3*). The A33 antigen is a member of the immunoglobulin superfamily, with homology to cell adhesion and tight junction–associated proteins (*4,5*). The antigen has been purified from human colon cancer cells, the protein sequence determined, the complementary DNA cloned, and the mouse homolog identified (*4,6*). Because of its restricted tissue localization and high level of expression, the A33 antigen is appealing as a therapeutic target, and a variety of anti-A33–based approaches are under preclinical investigation as potential therapies for colon cancer (*7–11*).

Early clinical studies (*12,13*) were performed with murine anti-A33 monoclonal antibody radiolabeled with ^{131}I or ^{125}I to assess its potential for radioimmunotherapy. Among the findings of these studies was that antibody localization at primary and metastatic tumor sites was extremely persistent, with significant retention beyond 6 wk after administration, whereas the initially high uptake in normal intestine gradually diminished with time. The applicability of murine A33 was restricted by the development of an antimouse IgG immune response and, in an attempt to overcome this limitation, a fully humanized complementarity determining region-grafted A33 IgG1 (huA33) was developed (*14*). However, subsequent studies showed that repetitive administrations of huA33 could elicit a human antihuman antibody response (*15*). Humanized antibody A33 (huA33) has been shown to be equivalent to the mouse antibody in competitive binding assays and localization studies in animal models (*14*) and can be radioiodinated with retention of immunoreactivity.

The relatively long half-life (4.2 d) of ^{124}I allows PET to be performed for up to a week after the administration of ^{124}I-labeled antibody (*16*), with radiation doses to normal tissues comparable with those of the ^{131}I-labeled antibody. It has been shown that quantitative noninvasive imaging of ^{124}I is possible using a dedicated PET system (*17,18*).

We performed a clinical study of ^{124}I-huA33 PET in patients with colorectal cancer. In 15 patients, for whom surgery was prescheduled as a standard of care, a PET/CT scan was acquired approximately 1 wk after antibody admin-

Received Jul. 11, 2011; revision accepted Sep. 9, 2011.
For correspondence or reprints contact: Joseph A. O'Donoghue, Department of Medical Physics, Memorial Sloan-Kettering Cancer Center, 1275 York Ave., New York, NY 10065.
E-mail: odonoghj@mskcc.org
Published online Nov. 8, 2011.

istration, immediately before the surgical removal of tumor and elements of neighboring normal tissues. Surgically excised tissues were subsequently processed for ex vivo quantification of antibody uptake, antigen density determination, digital autoradiography (DAR), and histologic or immunohistochemical staining. In this paper, we describe the findings of this study, focusing on the ex vivo measurements and their clinical implications. The clinical PET/CT is described only to the extent that it has an impact on these. A more comprehensive description of the clinical imaging study of ^{124}I-huA33 is provided elsewhere (*19*).

MATERIALS AND METHODS

Clinical Study with ^{124}I-huA33

Under the auspices of a protocol approved by the Institutional Review Board and an Investigational New Drug application approved by the Food and Drug Administration, 15 patients (mean age, 66 y; range, 52–77; 11 men, 4 women) with colorectal cancer were intravenously administered 10 mg of huA33 labeled with ^{124}I after providing informed consent (Trial registration ID, NCT00199862). On average, the administered activity was 200 MBq (5.4 mCi), and the range was 44–400 MBq (1.2–10.7 mCi). There were no adverse events related to huA33 administration for any patient in the study. Patients were imaged by PET/CT approximately 7 d later (range, 5–9 d) and underwent prescheduled surgery thereafter. Tumor and normal tissue samples were obtained at the time of surgery, as part of the standard of care, and portions of these were used in the analysis.

Antibody Radiolabeling

For clinical PET/CT, huA33 antibody was radiolabeled with ^{124}I, in accordance with USP <797> (*20*), using the IODO-GEN (Pierce) method (*21*). ^{124}I was either prepared by an in-house cyclotron (TR14/4; Ebco) or purchased commercially (IBA Molecular). Details of the labeling procedure are provided in the supplemental data (available online only at http://jnm.snmjournals.org). The average radiochemical yield was 92% ± 6% and, after ion exchange purification, the mean radiochemical purity was 98% ± 1%. Endotoxin levels were consistently below 0.4 EU/mL, all solutions were sterile, and the average immunoreactivity of the ^{124}I-huA33 was 90% ± 5%.

For ex vivo saturation binding studies, huA33 antibody was radiolabeled with ^{131}I purchased commercially (Nordion) using the IODO-GEN method (*21*) to a specific activity of 220–260 MBq/mg (6–7 mCi/mg). Details of the labeling procedure are provided in supplemental data. The radiochemical yield was greater than 90%, and ^{131}I-huA33 was more than 99% pure.

Tissue Sample Processing

Tissue samples recovered from surgery were divided into portions for γ-well counting and subsequent antigen density determination as well as DAR and tissue staining analysis.

Antigen Density Determination by Saturation Binding Analysis. Tissue samples were weighed, snap-frozen in liquid nitrogen, and immediately counted in a γ-well counter, together with appropriate ^{124}I standards. These were then stored at −80°C for 2 mo to allow decay of ^{124}I. Thereafter, tissue was thawed on ice, diced, put into 20 mM *N*-(2-hydroxyethyl)piperazine-*N*′-(2-ethanesulfonic acid)-KOH buffer (pH 7.4), and homogenized on ice with 4 × 10 s 24,000-rpm bursts with a disperser (T18 Basic ULTRA-TURRAX; IKA). Membranes were isolated by centrifugation at 5,000*g* for 20 min at 4°C and resuspended in phosphate-buffered saline using a Potter-Elvehjem tissue grinder. The protein content of membrane preparations was assayed using bicinchoninic acid reagent (Pierce) and measuring the absorption of the Cu(I) complex at 540 nm.

Saturation studies used 50–100 μg of membranes in phosphate-buffered saline incubated with increasing amounts of ^{131}I-huA33. Mixtures were incubated at room temperature for 60 min before rapid filtration through a glass fiber filter (GF/C; Whatman) presoaked in 1% bovine serum albumin/10 mM Tris-HCl (0.85% NaCl, pH 7.4). Filters were washed with 4 × 1 mL of ice-cold 10 mM Tris-HCl (0.85% NaCl, pH 7.4) and counted with a NaI (Tl) well scintillation counter. Each assay was performed in triplicate. Nonspecific binding was defined as that observed in the presence of 100 nM unlabeled huA33. The saturation binding data were evaluated using the least-squares fitting routine of the computer program Origin (version 7.5; Microcal Software) and by Scatchard transformation of the data. The maximum number of binding sites (B_{max}) and dissociation constant (K_d) values were obtained for all tissue samples, with the consistency of the K_d value acting as an experimental control.

DAR and Tissue Staining Analysis. Tissue samples for DAR and tissue staining analysis were individually wrapped in a layer of heavy-duty clear plastic wrap film and immersed into prechilled methylbutane (Fisher Scientific) at −80°C for 10 min. The frozen tissues were then embedded in optimal-cutting-temperature (OCT) compound (VWR Scientific) on dry ice and transferred to a −80°C freezer for 30 min. Sets of (typically 10) contiguous frozen 8-μm-thick sections were cut from each tissue sample using a HM500 cryostat microtome (Microm) and collected on glass microscope slides.

Adjacent tissue sections from the same contiguous set were used for DAR and for histologic and immunohistochemical staining.

A minimum of 3 frozen tissue sections from each specimen were placed in a film cassette against a Fujifilm BAS-MS2325 imaging plate (Fuji Photo Film Co.). Latent images were read out after variable exposure times (mean, 61 h; range, 18–165 h) using a Fujifilm BAS-1800II Bio-Imaging Analyzer (Fuji Photo Film Co.) at a 50-μm-pixel resolution. DAR image intensity was characterized by the machine readout parameter of photostimulable luminescence per square millimeter (PSL/mm^2). DAR calibration studies were performed to relate PSL/mm^2 to cumulated activity concentration (MBq h/mL). ^{124}I-huA33 uptake was derived from region-of-interest (ROI) analysis of the DAR images using Multi Gauge software (version 2.2; Fujifilm). ROIs were drawn to encompass entire tissue sections to facilitate comparison with the well counter measurements of tissue blocks. In addition, ROIs were drawn around identifiable zones in the DAR images, which were subsequently related to the histologic features of the tissue sections.

For conventional morphologic assessment, tissue sections were fixed in 10% phosphate-buffered formalin solution (15 min), washed with phosphate-buffered solution, and stained with hematoxylin and eosin (Sigma-Aldrich Inc.).

For immunohistochemical detection of A33 antigen, tissue sections were fixed in 10% neutral-buffered formalin (5 min), endogenous peroxidase was suppressed with H_2O_2, and a protein block for the reduction of nonspecific staining was applied. Thereafter murine monoclonal antibody A33 was applied at a concentration of 0.5 μg/mL overnight at 4°C. Primary antibody was detected using biotinylated horse antimouse-secondary reagent (1:200; Vector Labs), followed by avidin-biotin-complex system (ABC-Elite; Vector Labs) with 3′-3′-diaminobenzidine (DAB; Biogenex) as a chrom-

ogen. Sections were counterstained with hematoxylin. Negative control slides, omitting the primary antibody, were included in all assays. Images of stained sections were obtained with a BX600 digital microscope (Olympus).

DAR System Calibration

The DAR system response was calibrated using ^{124}I activity standards. Standards were constructed by mixing known activities of ^{124}I in known volumes of OCT compound. Uniform mixing was facilitated by including red food dye in the diluent and heating the OCT compound to 80°C. Subsequently, the activity-containing OCT compound was poured into moulds and frozen on dry ice. Sections of 8-μm thickness were cut and collected on glass microscope slides in a manner identical to that for the clinical specimens. At least 3 sets of serially diluted activity-containing sections were then exposed to imaging plates for times ranging from 5 to 116 h before being read out. ROIs were drawn on the images of the activity standards, interior to the visible edges, and over a background location. The signal from the activity standards was quantified in terms of mean background-corrected PSL/mm^2.

The cumulated activity concentration in a standard, $\tilde{a}_s$, was calculated by:

$$\tilde{a}_s = \int_0^{T_{exp}} a_{s0} exp(-\lambda t) dt = a_{s0}\left(1 - exp\left(-\lambda T_{exp}\right)\right)/\lambda,$$

where a_{s0} was the activity concentration in the standard at the beginning of the exposure, of duration T_{exp}, and λ was the physical decay constant of ^{124}I (0.00692 h^{-1}).

This procedure enabled the DAR system to be calibrated in terms of photostimulable luminescence per unit area per unit cumulated activity concentration (PSL/mm^2 per MBq h/mL).

DAR-Derived Fractional Tissue Uptake per Unit Volume

For clinical tissue samples, values of cumulated activity per unit volume were determined from ROI analysis of the DAR images using the system calibration factor. The implied activity concentrations at the beginning of the exposure were then compared with the total activity administered, corrected for decay to the beginning of the exposure, to derive fractional uptake per unit volume—that is:

$$F_{ROI} = a_{on\ ROI}/A_{on},$$

where F_{ROI} was the fractional uptake per unit volume in the ROI, $a_{on\ ROI}$ was the activity concentration in the ROI at the beginning of the DAR exposure, and A_{on} was the total administered activity corrected for decay to the beginning of the DAR exposure.

In terms of known or directly measured parameters:

$$F_{ROI} = \frac{\lambda \tilde{a}_{ROI}}{A_0 exp(-\lambda T_{on})\left(1 - exp\left(1 - \lambda T_{exp}\right)\right)},$$

where A_0 was the total administered activity, and T_{on} was the time between the administration of activity and the beginning of the DAR exposure of duration T_{exp}.

Statistical Analysis

Bivariate relationships were assessed by linear regression analysis. Differences between regression coefficients (m_1, m_2) were compared using the Student t test on the test statistic $t = (m_1 - m_2)/s_{m_1 - m_2}$, where $s_{m_1\ -\ m_2}$ is the SE of the difference between regression coefficients according to Chapter 18 of Zar (*22*). SD and SE are used to denote standard deviation and standard error, respectively.

RESULTS

Clinical PET/CT Images of ^{124}I-huA33

PET/CT images of ^{124}I-huA33 were generally of sufficiently high quality for diagnostic interpretation at approximately 1 wk after administration (*19*). Examples of such images are provided in Figures 1 and 2. The ^{124}I-huA33 maximum-intensity-projection images (Figs. 1C and 2C) indicate the presence of activity primarily in A33-expressing tissue but also in the circulation (cardiac blood pool and blood vessels). Although the entire intestinal tract was clearly visualized, little activity was present in any other parenchymal or connective tissue. The axial PET/CT images (Figs. 1D and 2D) show focal ^{124}I-huA33 uptake in primary and metastatic tumor and also normal colon.

Patterns of ^{124}I-huA33 Uptake in Clinical Tissue Sections

Twenty-nine tissue samples from 14 patients were evaluable by DAR, including both tumor (*16*) and nontumor (*13*) material. Figures 1E–1J show a set of DAR and hematoxylin and eosin–stained sections of tissues surgically removed after acquisition of the ^{124}I-huA33 clinical images shown in Figures 1C and 1D. Focal uptake was apparent in regions of viable tumor cells with little uptake in tumor-infiltrating stroma. The DAR images also show high uptake in normal colonic mucosa, consistent with the known expression pattern of A33 antigen (*1–3*), with relatively low uptake in liver. ROIs drawn on the DAR around the whole tumor tissue section and around several of the focal high-activity zones indicated that the whole-section average uptake of 0.025 percentage injected dose per milliliter (%ID/mL) was considerably less than that in the focal regions (~0.10 %ID/mL).

Figures 2E–2G show another tumor tissue section image set (contiguously aligned sections assessed by DAR, hematoxylin and eosin staining, and immunohistochemistry staining for A33 antigen). Comparison of these images indicates that the distribution of ^{124}I-huA33 conformed closely to viable antigen-positive tumor. ROI analysis indicated that the average section uptake (0.018 %ID/mL) was considerably less than that in viable antigen-positive tumor regions (~0.044 %ID/mL).

Table 1 summarizes the DAR-based measurements for all patients studied in terms of ^{124}I-huA33 uptake expressed in %ID/mL. Section average and regional (i.e., antigen-positive) uptake from up to 2 separate tumor locations were examined together with normal colonic mucosa if available. Noncolon normal tissues generally had low uptake as exemplified by the lymphoid tissue samples for patients 10 and 12 (0.003 %ID/mL) and by the normal liver sample shown in Figures 1G and 1J) (0.002 %ID/mL) for patient 15 (not included in table). Table 1 indicates that the uptake of

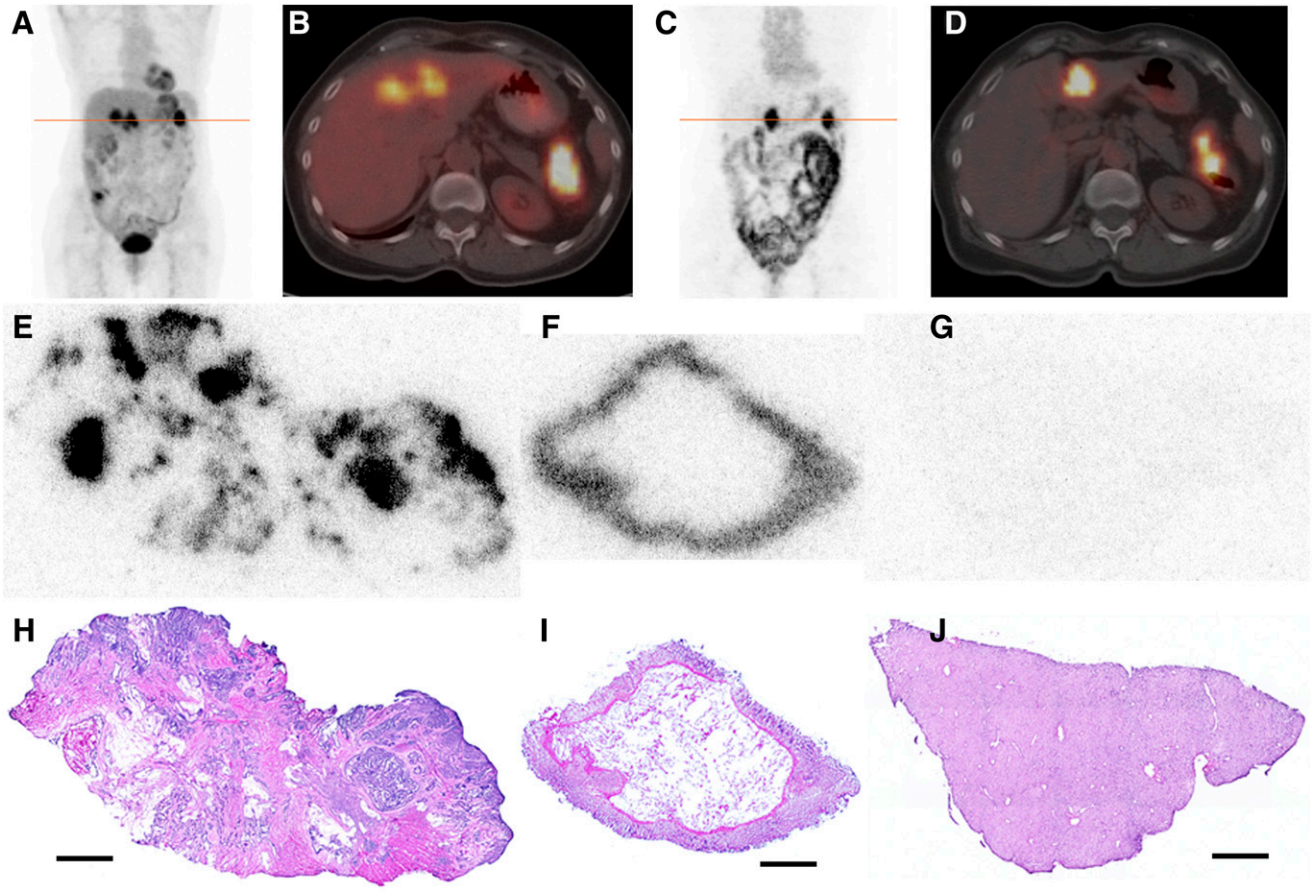

FIGURE 1. (A–B) ^{18}F-FDG PET/CT scan acquired immediately before administration of ^{124}I-huA33: coronal maximum-intensity-projection image (A) and transaxial PET/CT slice (B) through line of A. Images show pathologic uptake in primary (splenic flexure of colon) and metastatic (liver) lesions together with normal physiologic accumulation. (C–D) Clinical PET/CT scan acquired 162 h after administration of 395 MBq (10.7 mCi) of ^{124}I-huA33: coronal maximum-intensity-projection (C) and transaxial PET/CT slice (D) through line of C. Intense focal uptake is visible in primary and metastatic tumor together with significant uptake throughout normal intestine. (E–J) DAR (E–G) and hematoxylin and eosin–stained (H–J) tissue sections corresponding to features observed in clinical image: primary tumor (E and H), normal colon (F and I), and normal liver (G and J). In tumor section, ^{124}I-huA33 is localized primarily in regions of viable tumor cells with little stromal uptake. Normal colonic mucosa has high and uniform uptake. Little to no uptake is present in normal liver. Scale bars = 2 mm.

huA33 in colon cancer was generally high and that uptake in regions of viable tumor (mean ± SE, 0.052 ± 0.007 %ID/mL) was significantly greater than section average values (mean ± SE, 0.019 ± 0.003 %ID/mL). Uptake in colonic mucosa was also high (mean ± SE, 0.03 ± 0.01 %ID/mL).

Antigen Density Determination by Saturation Binding Analysis

Figure 3A shows an example of a saturation binding curve for membranes derived from a homogenized tumor sample. In general, saturation binding data were typical of a single binding interaction, with K_d values for all studies approximately similar (mean ± SD, 0.52 ± 0.15 nM). Figures 3B and 3C show, respectively, tumor and colon B_{max} values, derived from all clinical tissue samples analyzed, plotted against the corresponding well counter–measured ^{124}I-A33 uptake. For both tumor and normal colon, these relationships appear linear, although with greater variability in the case of the colon (r^2 = 0.40 vs. 0.75 for tumor). The best-fitting slope of B_{max} versus uptake for tumor samples (mean ± SE, 59 ± 7 pmol/mg/%ID/g) was less steep ($P < 0.01$) than that for colon samples (mean ± SE, 97 ± 25 pmol/mg/%ID/g).

These data were used to estimate binding site occupancy for tumor and colon, assuming that no antigen degradation occurred in storage and that bound antibody at the time of surgery remained bound at the time of assay. The occupancy, O (i.e., ratio of bound antibody to total antigen), is given by:

$$O = C_{ab}/(C_{ab} + C_{ag}) = 1/(1 + (C_{ag}/C_{ab})),$$

where C_{ab} and C_{ag} are the respective concentrations of bound antibody and free antigen (i.e., that determined by saturation binding assay), respectively. To provide representative estimates of occupancy factor, independent of the level of antibody binding, regression coefficients were recalculated for through-origin fits of A33 sites versus ^{124}I-huA33 uptake. This yielded values of 77 and 110 pmol/mg

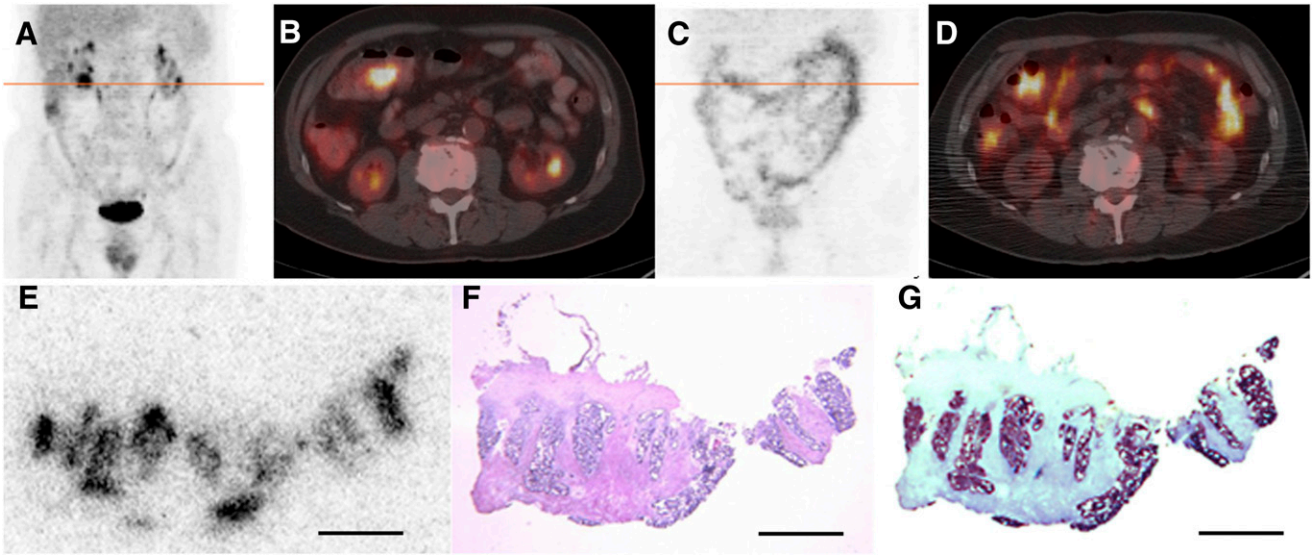

FIGURE 2. (A–B) ^{18}F-FDG PET/CT scan acquired immediately before administration of ^{124}I-huA33 shows pathologic uptake in lesion in transverse colon near hepatic flexure together with normal physiologic accumulation. (C–D) PET/CT scan acquired 182 h after administration of 140 MBq (3.8 mCi) of ^{124}I-huA33 shows focal uptake in tumor (compare B and D) and throughout normal intestine. (E–G) Contiguously aligned sections of tumor visualized in D assessed by ^{124}I-DAR (E), hematoxylin and eosin staining (F), and immunohistochemical staining (G) for A33 antigen. ^{124}I-huA33 localized only in small (~1 mm in dimension) regions of viable antigen-positive tumor and not in antigen-negative stroma. Scale bars = 2 mm.

of membrane per %ID/g of tissue for tumor and colon, respectively. For the membrane recovery observed (10–20 mg of membrane per gram of tissue), the free antigen–to–antibody ratio was thus 770–2,200 pmol of antigen/670 pmol of antibody (1% of 10 mg of a 150-kDa antibody = 670 pmol), resulting in occupancy factors in the range 0.23–0.46. This range implies that approximately 20%–50% of A33 binding sites in tumor and colonic mucosa were occupied.

Comparative Well Counter and DAR Measurements

Figure 4 plots average ^{124}I-huA33 uptake in tissue sections estimated by DAR analysis versus well counter–derived uptake for corresponding tissue specimens. Although the tissue sections and specimens for well counting were derived from different portions of the resected tissue samples and the DAR-based estimates were based on a relatively small number (typically 4) of 8-μm-thick tissue sections (directly accounting for only a small proportion of the total volume), there was a linear relationship ($r^2 \sim 0.6$) between uptake values with a best-fitting straight line close to the line of identity.

DISCUSSION

We observed linear relationships between antigen concentration and ^{124}I-huA33 uptake in both tumor and normal

TABLE 1
Summary of DAR Measurements (%ID/mL) on Tissue Sections Cut from Surgically Removed Material

Patient no.	Time after injection* (d)	Tumor 1	Tumor 1 regional	Tumor 2	Tumor 2 regional	Normal	Normal tissue type
2	5	0.015	0.040	0.026	0.096	0.010	Normal colon
3	6	0.015	0.050	—	—	0.017	Normal colon
4	8	0.018	0.044	—	—	—	—
5	7	0.008	0.021	—	—	0.009	Normal colon
6	7	0.030	0.057	0.029	0.046	0.006	Normal colon
7	6	0.058	0.113	—	—	0.034	Normal colon
8	6	0.017	0.054	—	—	0.012	Normal colon
9	6	0.004	0.036	—	—	—	—
10	7	0.004	0.011			0.003	Lymphoid tissue
11	7	—	—			0.075	Normal colon
12	7	0.014	0.029	0.017	0.043	0.003	Lymphoid tissue
13	7	0.012	0.030			0.009	Normal colon
14	9	—	—			0.093	Normal colon
15	7	0.025	0.102	0.016	0.067	0.039	Normal colon

*Time between antibody administration and surgery.

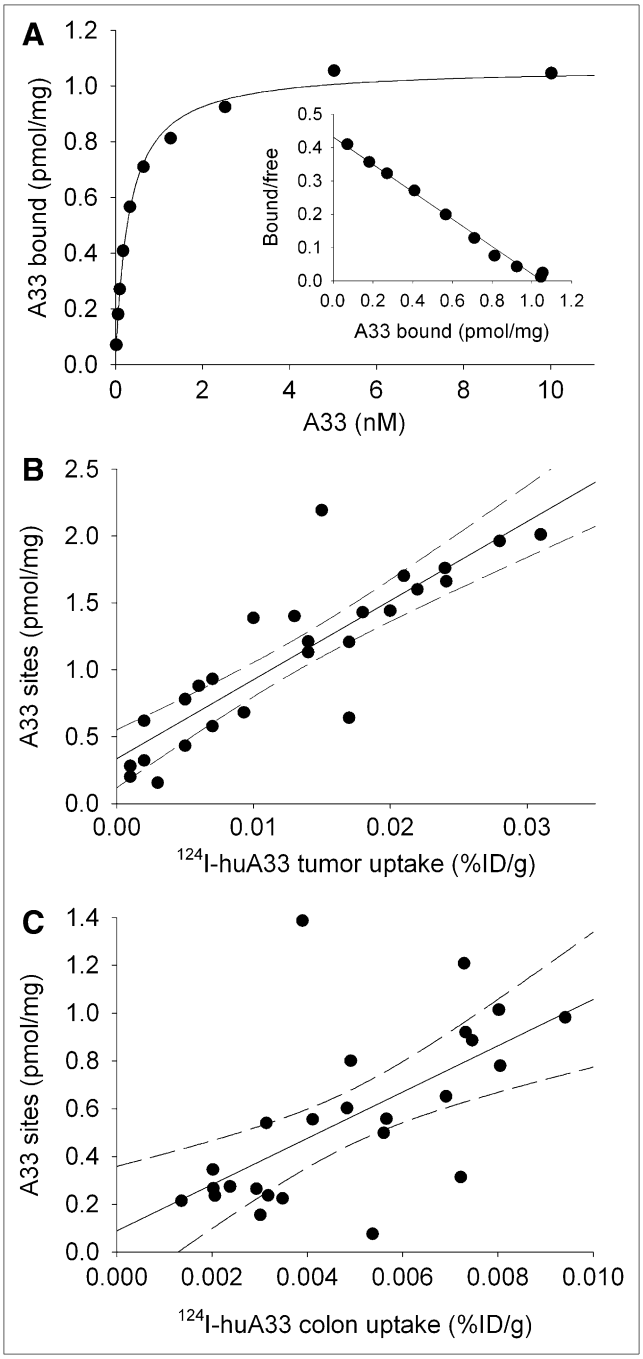

FIGURE 3. (A) Example of A33 saturation binding curve for membranes derived from surgically removed tumor sample together with Scatchard transformed data plot (insert). Mean K_d ± SE, 0.31 ± 0.02 nM; mean B_{max} ± SE, 1.07 ± 0.02 pmol/mg. (B) Scatterplot of A33 antigen density for membranes derived from tumor homogenates vs. ^{124}I-huA33 uptake as determined by well counter measurements. Predicted 95% confidence limits are shown as dashed lines. Regression equation, y = 59 (SE, 7)x + 0.3 (SE, 0.1) (n = 26; r^2 = 0.75). (C) Scatterplot of A33 antigen density for membranes derived from normal colon homogenates vs. ^{124}I-huA33 uptake determined by well counter measurements. Regression equation, y = 97 (SE, 25)x + 0.09 (SE, 0.1) (n = 25; r^2 = 0.40).

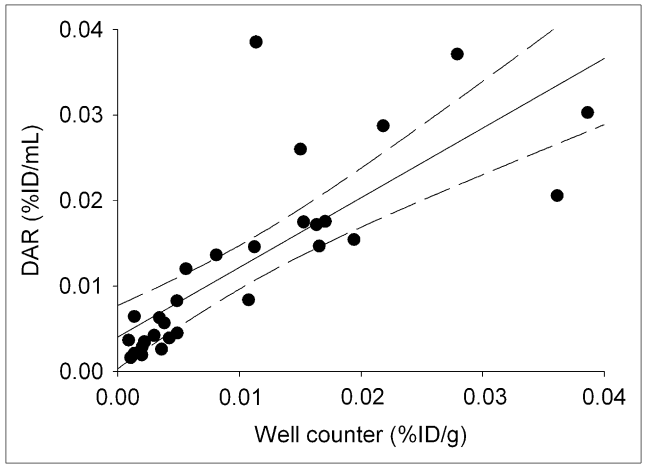

FIGURE 4. Scatterplot of tissue %ID/mL estimated using DAR vs. well counter measurements (%ID/g) of intact tissue samples. Regression equation, y = 0.81 (SE, 0.12)x + 0.004 (SE, 0.002) (n = 29; r^2 = 0.62).

colon. The steeper slope for colon may be due to the process of cellular turnover. Previous studies have shown high and uniform expression of A33 antigen throughout the intestinal epithelium from crypt to villi (*1,6*). During the period between antibody administration and surgery, mature epithelial cells (together with any associated antibody) will be shed into the intestinal lumen in a normal physiologic process. Concurrently, circulating antibody will continue to bind but at a decreasing rate in line with the decreasing plasma concentration of antibody—together, these are predicted to lead to a slowly diminishing ratio of antibody-to-antigen concentration. This is discussed in more detail in supplemental data.

The study findings have implications for the use of huA33 as a molecular vector for radionuclide therapy of colon cancer. The average tumor uptake (0.017 or 0.019 %ID/mL by well counter or DAR-based measurements, respectively) is among the highest reported for radiolabeled antibodies. Furthermore, as illustrated by the histologic images, antigen-positive tumor cells typically comprise only a fraction of bulk resected tumor samples. The DAR-based measurements show that huA33 uptake in regions of antigen-positive tumor was approximately 3 times greater than whole-section averages (0.052 vs. 0.019 %ID/mL), implying that, at the microscopic level, radiation doses delivered to tumor cells may be significantly greater than tissue average–based estimates would suggest. The antigen-positive tumor regions seen on histologic images were typically of 1–2 mm in dimension. For high-energy/long-range β-emitters (e.g., ^{90}Y), only a small fraction (~10%) of the emitted energy would be absorbed in regions of this size whereas the rest would be deposited in the surrounding stroma (*23–25*). In contrast, for lower-energy/shorter-range β-emitters (e.g., ^{177}Lu), a much greater proportion of the emitted β-energy would be absorbed locally (*24,25*), suggesting that radionuclides with shorter emission ranges would be preferable for the disease conformations observed.

The high uptake observed in normal colon is also an important factor for radionuclide therapy, because enhanced radiation dose to the gut could result in toxicity. It is, however, significant that gut toxicity has not been observed in previous radioimmunotherapy studies using ^{131}I- or ^{125}I-labeled anti-A33 antibody (*12,13,26*).

Welt et al. (*12*) found that the maximally tolerated activity for ^{131}I-A33 (i.e., the original murine antibody) was 2.8 GBq/m^2 (75 mCi/m^2). Chong et al. (*26*), using ^{131}I-huA33 (i.e., the complementarity determining region-grafted humanized antibody), found a reduced maximally tolerated activity of 1.5 GBq/m^2 (40 mCi/m^2). This difference probably reflects pharmacokinetic differences between murine and humanized antibodies, but in both cases hematologic toxicity was dose-limiting. The most likely reason gut toxicity was not previously observed is simply that the amount of ^{131}I-huA33 required to produce it was less than that which produced dose-limiting hematologic toxicity. This is partly because the hemopoietic system is more radiosensitive than the gut and partly because a large fraction (~70%) of the decay energy of ^{131}I is emitted in the form of long-range γ-rays, which disperse the energy throughout the body, thereby reducing the dosimetric selectivity between high- and low-antigen-density regions. The use of alternative radionuclides that lack significant long-range photon emission (e.g., ^{90}Y, ^{177}Lu) would be expected to increase the relative clinical impact of gut toxicity.

For radioimmunotherapy with ^{125}I-A33, activities of up to 13 GBq/m^2 (350 mCi/m^2) were administered without reaching maximally tolerated activity (*13*), suggesting that neither the antigen-negative cells of the hemopoietic system nor the antigen-positive cells of the intestine experienced significant radiobiologic effects from the highly localized Auger electron emissions of ^{125}I. This may reflect noninternalization of A33 antigen in the cells of the intestinal epithelium as has recently been described for A33-expressing cells in culture (*5*).

Interestingly, the study of ^{125}I-A33 (*13*) also showed extremely persistent antibody localization at primary and metastatic tumor sites, with significant retention beyond 6 wk after administration, whereas intestinal activity cleared by 7–8 d after administration. In the current study, we observed significant huA33 antibody uptake in antigen-positive colon at approximately 7 d after administration, as was also observed by Scott et al. (*27*). The discrepancy between our observations and those of Welt et al. may be due to slower plasma clearance of humanized (vs. murine) antibody, which would extend the time of availability for binding to antigen-positive cells in the intestine.

The results of this study, together with previous findings, suggest 2 features of an optimal radioimmunotherapy strategy based on the A33 system. First, the optimal therapeutic radionuclide is likely to be a short-range (α- or β-particle) emitter with limited long-range (β-particle or γ/x-ray) emission. Second, the observation of high antibody uptake in antigen-positive gut that decreases slowly, coupled with persistent antibody retention in tumor, suggests that a multistep approach would be advantageous. Multistep (*28–31*) refers to a treatment strategy based on the initial administration of an unlabeled antibody-based molecular construct with additional specificity for some small molecule, followed at a later time by the administration of the small molecule labeled with a suitable radionuclide. Selectivity is achieved by administering the radiolabel only after the antibody construct has cleared from nontumor sites. This process may be accelerated by the use of a clearing agent to remove the antibody construct from the circulation (*29,30*). An illustration of the potential advantages of a multistep approach, based on a model simulation, is provided in supplemental data.

Although earlier studies (*32*) suggested that the A33 antibody–antigen complex was internalized, more recent work indicates that the antigen appears to colocalize with tight junction proteins and largely escapes endocytosis (*5*). Moreover, even in cases in which antibodies are known to have some degree of internalization, multistep approaches may show improved efficacy (*33,34*). In such circumstances, the extent and rate of internalization will be important determinants of utility. For a multistep approach, normal tissue side effects would be determined not by the biodistribution and pharmacokinetics of a large molecule but by those of a small rapidly clearing one. A multistep approach would be expected to increase the relative significance of the kidney as a dose-limiting organ (*35,36*). We are currently investigating the feasibility of multistep targeting approaches based on the A33 system.

CONCLUSION

We found that the spatial distribution of huA33 antibody conformed to that of A33 antigen in tissues from patients with colorectal cancer who had been imaged by ^{124}I-huA33 immuno-PET and that there was a linear relationship between antibody concentration and antigen density. These findings support the concept that late PET of ^{124}I-huA33 antibody can provide a map of A33 antigen density. Antibody uptake in regions of antigen-positive tumor cells was typically high (mean, ~0.05 %ID/g), with high uptake also observed in antigen-positive normal colon. We anticipate that the optimal strategy for radioimmunotherapy, based on the A33 system, will be a multistep treatment using a short-range radionuclide.

DISCLOSURE STATEMENT

The costs of publication of this article were defrayed in part by the payment of page charges. Therefore, and solely to indicate this fact, this article is hereby marked "advertisement" in accordance with 18 USC section 1734.

ACKNOWLEDGMENT

This work was supported by NIH grant PO1 CA33049 and by the Ludwig Center for Cancer Immunology (LCCI) at Sloan-Kettering Institute (SKI). No other potential conflict of interest relevant to this article was reported.

REFERENCES

1. Garinchesa P, Sakamoto J, Welt S, Real FX, Rettig WJ, Old LJ. Organ-specific expression of the colon cancer antigen A33, a cell surface target for antibody-based therapy. *Int J Oncol.* 1996;9:465–471.
2. Johnstone CN, White SJ, Tebbutt NC, et al. Analysis of the regulation of the A33 antigen gene reveals intestine-specific mechanisms of gene expression. *J Biol Chem.* 2002;277:34531–34539.
3. Sakamoto J, Kojima H, Kato J, Hamashima H, Suzuki H. Organ-specific expression of the intestinal epithelium-related antigen A33, a cell surface target for antibody-based imaging and treatment in gastrointestinal cancer. *Cancer Chemother Pharmacol.* 2000;46:S27–S32.
4. Heath JK, White SJ, Johnstone CN, et al. The human A33 antigen is a transmembrane glycoprotein and a novel member of the immunoglobulin superfamily. *Proc Natl Acad Sci USA.* 1997;94:469–474.
5. Ackerman ME, Chalouni C, Schmidt MM, et al. A33 antigen displays persistent surface expression. *Cancer Immunol Immunother.* 2008;57:1017–1027.
6. Johnstone CN, Tebbutt NC, Abud HE, et al. Characterization of mouse A33 antigen, a definitive marker for basolateral surfaces of intestinal epithelial cells. *Am J Physiol Gastrointest Liver Physiol.* 2000;279:G500–G510.
7. Almqvist Y, Orlova A, Sjostrom A, et al. In vitro characterization of At-211-labeled antibody A33: a potential therapeutic agent against metastatic colorectal carcinoma. *Cancer Biother Radiopharm.* 2005;20:514–523.
8. Almqvist Y, Steffen AC, Tolmachev V, Divgi CR, Sundin A. In vitro and in vivo characterization of Lu-177-huA33: a radioimmunoconjugate against colorectal cancer. *Nucl Med Biol.* 2006;33:991–998.
9. Deckert PM, Bornmann WG, Ritter G, et al. Specific tumour localisation of a huA33 antibody: carboxypeptidase A conjugate and activation of methotrexate-phenylalanine. *Int J Oncol.* 2004;24:1289–1295.
10. Coelho V, Dernedde J, Petrausch U, et al. Design, construction, and in vitro analysis of A33scFv: CDy, a recombinant fusion protein for antibody-directed enzyme prodrug therapy in colon cancer. *Int J Oncol.* 2007;31:951–957.
11. Cortez C, Tomaskovic-Crook E, Johnston APR, et al. Influence of size, surface, cell line, and kinetic properties on the specific binding of A33 antigen-targeted multilayered particles and capsules to colorectal cancer cells. *ACS Nano.* 2007;1:93–102.
12. Welt S, Divgi CR, Kemeny N, et al. Phase I/II study of iodine 131-labeled monoclonal-antibody A33 in patients with advanced colon-cancer. *J Clin Oncol.* 1994;12:1561–1571.
13. Welt S, Scott A, Divgi C, et al. Phase I/II study of iodine 125-labeled monoclonal antibody A33 in patients with advanced colon cancer. *J Clin Oncol.* 1996;14:1787–1797.
14. King DJ, Antoniw P, Owens RJ, et al. Preparation and preclinical evaluation of humanized A33 immunoconjugates for radioimmunotherapy. *Br J Cancer.* 1995;72:1364–1372.
15. Ritter G, Cohen LS, Williams C, Richards EC, Old LJ, Welt S. Serological analysis of human anti-human antibody responses in colon cancer patients treated with repeated doses of humanized monoclonal antibody A33. *Cancer Res.* 2001;61:6851–6859.
16. Divgi CR, Pandit-Taskar N, Jungbluth AA, et al. Preoperative characterisation of clear-cell renal carcinoma using iodine-124-labelled antibody chimeric G250 (I-124-cG250) and PET in patients with renal masses: a phase I trial. *Lancet Oncol.* 2007;8:304–310.
17. Pentlow KS, Graham MC, Lambrecht RM, Cheung NKV, Larson SM. Quantitative imaging of I-124 using positron emitting tomography with applications to radioimmunodiagnosis and radioimmunotherapy. *Med Phys.* 1991;18:357–366.
18. Pentlow KS, Graham MC, Lambrecht RM, et al. Quantitative imaging of iodine-124 with PET. *J Nucl Med.* 1996;37:1557–1562.
19. Carrasquillo JA, Pandit-Taskar N, O'Donoghue JA, et al. ^{124}I-huA33 antibody PET of colorectal cancer. *J Nucl Med.* 2011;52:1173–1180.
20. United States Pharmacopeial Convention, Inc. *Pharmaceutical compounding–sterile preparations. USP <797>. First Supplement to The United Stated Pharmacopeia, 27th rev.; and The National Formulary, 22nd ed*. Rockville, MD: United States Pharmacopeial Convention, Inc.; 2004.
21. Fraker PJ, Speck JC. Protein and cell-membrane iodinations with a sparingly soluble chloramide, 1,3,4,6-tetrachloro-3A,6A-diphenylglycoluril. *Biochem Biophys Res Commun.* 1978;80:849–857.
22. Zar JH. *Biostatistical Analysis*. Fifth ed. Upper Saddle River, NJ: Prentice Hall; 2010.
23. Humm JL. Dosimetric aspects of radiolabeled antibodies for tumor therapy. *J Nucl Med.* 1986;27:1490–1497.
24. Bardiès M, Chatal JF. Absorbed doses for internal radiotherapy from 22 beta-emitting radionuclides - beta-dosimetry of small spheres. *Phys Med Biol.* 1994;39:961–981.
25. O'Donoghue JA, Bardiès M, Wheldon TE. Relationships between tumor size and curability for uniformly targeted therapy with beta-emitting radionuclides. *J Nucl Med.* 1995;36:1902–1909.
26. Chong G, Lee F, Hopkins W, et al. Phase I trial of I-131-huA33 in patients with advanced colorectal carcinoma. *Clin Cancer Res.* 2005;11:4818–4826.
27. Scott AM, Lee FT, Jones R, et al. A phase I trial of humanized monoclonal antibody A33 in patients with colorectal carcinoma: Biodistribution, pharmacokinetics, and quantitative tumor uptake. *Clin Cancer Res.* 2005;11:4810–4817.
28. Boerman OC, van Schaijk FG, Oyen WJG, Corstens FHM. Pretargeted radioimmunotherapy of cancer: Progress step by step. *J Nucl Med.* 2003;44:400–411.
29. Forero A, Weiden PL, Vose JM, et al. Phase 1 trial of a novel anti-CD20 fusion protein in pretargeted radioimmunotherapy for B-cell non-Hodgkin lymphoma. *Blood.* 2004;104:227–236.
30. Green DJ, Pagel JM, Pantelias A, et al. Pretargeted radioimmunotherapy for B-Cell lymphomas. *Clin Cancer Res.* 2007;13:5598s–5603s.
31. Gold DV, Goldenberg DM, Karacay H, et al. A novel bispecific, trivalent antibody construct for targeting pancreatic carcinoma. *Cancer Res.* 2008;68:4819–4826.
32. Daghighian F, Barendswaard E, Welt S, et al. Enhancement of radiation dose to the nucleus by vesicular internalization of iodine-125-labeled A33 monoclonal antibody. *J Nucl Med.* 1996;37:1052–1057.
33. Zhang M, Zhang Z, Garmestani K, et al. Pretarget radiotherapy with an anti-CD25 antibody streptavidin fusion protein was effective in therapy of leukemia/lymphoma xenografts. *Proc Natl Acad Sci USA.* 2003;100:1891–1895.
34. Sato N, Hassan R, Axworthy DB, et al. Pretargeted radioimmunotherapy of mesothelin-expressing cancer using a tetravalent single-chain Fv-streptavidin fusion protein. *J Nucl Med.* 2005;46:1201–1209.
35. Förster GJ, Santos EB, Smith-Jones PM, Zanzonico P, Larson SM. Pretargeted radioimmunotherapy with a single-chain antibody/streptavidin construct and radiolabeled DOTA-biotin: strategies for reduction of the renal dose. *J Nucl Med.* 2006;47:140–149.
36. O'Donoghue J. Relevance of external beam dose-response relationships to kidney toxicity associated with radionuclide therapy. *Cancer Biother Radiopharm.* 2004;19:378–387.

JNM The Journal of NUCLEAR MEDICINE

^{124}I-huA33 Antibody Uptake Is Driven by A33 Antigen Concentration in Tissues from Colorectal Cancer Patients Imaged by Immuno-PET

Joseph A. O'Donoghue, Peter M. Smith-Jones, John L. Humm, Shutian Ruan, Daniel A. Pryma, Achim A. Jungbluth, Chaitanya R. Divgi, Jorge A. Carrasquillo, Neeta Pandit-Taskar, Yuman Fong, Vivian E. Strong, Nancy E. Kemeny, Lloyd J. Old and Steven M. Larson

J Nucl Med. 2011;52:1878-1885.
Published online: November 8, 2011.
Doi: 10.2967/jnumed.111.095596

The Journal of Nuclear Medicine is published monthly.
SNMMI | Society of Nuclear Medicine and Molecular Imaging
1850 Samuel Morse Drive, Reston, VA 20190.
(Print ISSN: 0161-5505, Online ISSN: 2159-662X)

SNMMI SOCIETY OF NUCLEAR MEDICINE AND MOLECULAR IMAGING